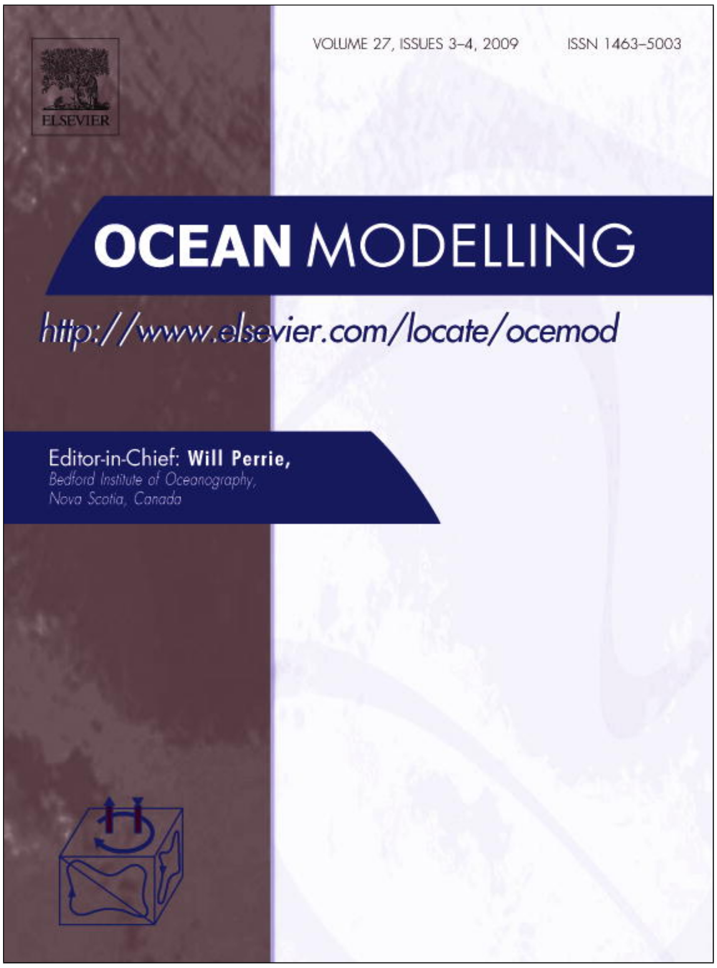
VOLUME 27, ISSUES 3–4, 2009
ISSN 1463-5003
ELSEVIER
OCEAN MODELLING
http://www.elsevier.com/locate/ocemod
Editor-in-Chief: Will Perrie,
Bedford Institute of Oceanography,
Nova Scotia, Canada

Ocean Modelling 27 (2009) 185–197

Contents lists available at ScienceDirect

Ocean Modelling

journal homepage: www.elsevier.com/locate/ocemod

Ekman drift and vortical structures

Yves Morel [a,*], Leif N. Thomas [b]

[a] SHOM (site de METEO-France), 42 Av. Gaspard Coriolis, 31057 Toulouse, France
[b] 473 Via Ortega Y2E2 Bldg., Stanford University MC 4215, Stanford, CA 94305-4215, USA

ARTICLE INFO

Article history:
Received 9 June 2008
Received in revised form 7 January 2009
Accepted 10 January 2009
Available online 19 January 2009

Keywords:
Vortex
Wind
Transport

ABSTRACT

In this article, the authors study the influence of a constant wind on the displacement of a vortex. The well known Ekman current develops in the surface layer and is responsible for a transport perpendicular to the wind: the Ekman drift.

An additional process is, however, evidenced, whose importance is as strong as the Ekman drift. There indeed exists a curl of the wind-driven acceleration along isopycnic surfaces when they are spatially variable (they enter and leave the depth where the wind stress acts), which generates potential vorticity anomalies. This diabatic effect is shown to generate potential vorticity anomalies which acts on the propagation of vortical waves and non linear vortices.

It is shown that this effect drastically reduces the effect of the Ekman drift for linear waves and surface intensified vortices, while extending its effect to subsurface vortices. It also generates along wind propagation, whose sign depends on the vortex characteristics.

1. Introduction

1.1. Ekman drift

The FRAM expeditions, directed by Fridtjof Nansen, aimed at reaching the North pole thanks to the drift of Nansen's boat "FRAM" with ice. During this expedition Nansen was the first to notice that the drift of ice and icebergs, which he associated with currents generated by the wind in the upper layers of the ocean, were not in the direction of the mean winds, but rather at an angle of 20–40° to the right of the wind.

The explanation of this observation was then proposed as a theoretical subject to Vagn Ekman by Vilhelm Bjerknes which resulted in the famous Ekman spiral theory and Ekman drift (Ekman (1905)), showing in particular that the mean transport over the upper layer affected by the wind stress is at the right and perpendicular to the wind, because of the Coriolis effect.

1.2. Advection of vortices by large scale currents

The dynamics of vortices has been the subject of many theoretical, numerical and observational studies in the past (see Carton (2001, 2008)). Observations have revealed that vortices were not merely advected by currents at the depth of their core (see Richardson et al. (1989)) and that more complicated mechanisms have to be invoked to explain the observed trajectories. The role of the planetary beta-effect has been studied by different authors (see for instance Sutyrin and Flierl (1994), Morel and McWilliams (1997), Sutyrin and Morel (1997), Ito and Kubokawa (2003), and references therein) and is able to explain part of the observed trajectories, but the influence of background currents has been invoked as a major mechanism for their propagation (see Dewar and Meng (1995)).

Hogg and Stommel (1990) were the first to propose a general theory for the interaction of vortices with large scale baroclinic currents: they showed that the mean propagation is an average of the current weighted by the potential vorticity anomaly (PVA) of the vortex. In their study, the authors have neglected the influence of the current PVA gradient, associated with the current vertical shear, and which can act as an additional beta-effect. This was shown to be non negligible as soon as the vortex radius is above the internal radius of deformation, which is often the case (see Morel (1995)). This was later studied in detail by Vandermeirsch et al. (2001) who showed that the beta-effect associated with the background current PVA gradient actually compensates the advective effect of the current. According to their theory, only the barotropic part of large scale currents should have an influence on the propagation of coherent vortices.

However, when large scale currents are associated with Ekman drift, they are intensified near the surface and are equilibrated by the wind stress. In this case they are not associated with PVA gradients and the compensation effect can thus play no role, so that we could expect Hogg and Stommel theory to apply here. Thus there should be a strong influence of the Ekman drift on the propagation of vortices, at least for surface intensified structures in regions where the wind is strong. For instance Dewar and Meng

* Corresponding author.
E-mail addresses: yves.morel@shom.fr (Y. Morel), leift@stanford.edu (L.N. Thomas).

1463-5003/$ - see front matter © 2009 Elsevier Ltd. All rights reserved.
doi:10.1016/j.ocemod.2009.01.002

(1995) considered a lens of intermediate water embedded between two layers in which a background current, generated by large scale winds in some more realistic experiments, was present. They found a strong influence of background currents on the propagation of vortices.

1.3. Present study: Influence of a wind stress on a vortex

Recently Thomas (2005) and Morel et al. (2006) have shown that a spatially constant wind stress can induce PV modifications at ocean fronts using different approaches. Thomas (2005) used a continuously stratified fluid, including a realistic mixed layer, for which surface fronts are associated with horizontal density gradients. He showed that, when such fronts are exposed to a spatially uniform wind, frictional PV fluxes are generated that result in the formation of PVAs (Thomas, 2005; Thomas and Ferrari, 2008). Morel et al. (2006) used an isopycnic model and showed that PVAs can be generated by winds when the vertical position of isopycnic surfaces varies. Indeed, potential vorticity has to be evaluated along isopycnic surfaces. If their vertical position varies, isopycnic surfaces can enter/leave the depth where the wind stress acts. Wind-driven acceleration can then vary along the isopycnic surfaces, and there can exist a curl giving rise to the generation of potential vorticity anomalies. This theory was applied to study the stability property of a coastal upwelling current, but Morel et al. (2006) identified the dynamics of vortices as another process for which the modification of PVA generated by the wind stress could play an interesting role.

This problem was first addressed by Stern (1965) who analysed the non-linear interactions between the Ekman flow – produced by a uniform wind stress – and a geostrophic vortex. He showed that a new term arises in the mixed layer vorticity equation when a pre-existing vortex is considered, which induces vortex propagation. Stern then calculated the propagation speed of small perturbations in a two-layer model and showed that short waves are advected by the mean Ekman drift but waves – or vortices – whose lengthscales are of the order or larger than the radius of deformation propagate more slowly.

We here revisit this problem and we perform numerical simulations, using a two layer configuration, to confirm Stern's analysis and sensitivity studies to complement it. We also propose a new theoretical approach to analyse the mechanisms at stake, based on the development of the beta-gyre (see Sutyrin and Flierl (1994)), that is able to explain the observed behavior and some new effects (such as along wind propagation and influence on deep vortices).

The second section describes the equations and configuration considered here. The third section presents results for a reference experiment. A theoretical analysis is proposed in the fourth section and the fifth one is devoted to sensitivity studies to the vortex and background stratification characteristics. The last section sums up our results and discusses possible applications and extensions.

2. Equations and generalities

2.1. Equations

We consider a two-layer, adiabatic shallow water model (see Bleck and Boudra (1986), Pedlosky (1987), Cushman-Roisin (1994)) satisfying:

$$\partial_t U_k + (\vec{U_k}.\vec{\nabla})U_k - fV_k = -\partial_x M_k$$
$$\partial_t V_k + (\vec{U_k}.\vec{\nabla})V_k + fU_k = -\partial_y M_k + T_y^w \delta_{k,1}$$
$$\partial_t h_k + div(h_k \vec{U_k}) = 0. \tag{1}$$

Here $\vec{U_k} = (U_k, V_k)$ is the horizontal velocity field, $f = 1 \times 10^{-4} s^{-1}$ is the Coriolis frequency (which we assume to be spatially constant in this paper), h_k is the thickness of an isopycnal layer, $k = 1, 2$ is the layer index and M_k is the Montgomery potential which is given by:

$$M_1 = g\eta$$
$$M_2 = M_1 - g' h_1, \tag{2}$$

where η is the sea-surface elevation, $g = 9.806\ \mathrm{m/s^2}$ is the gravity, and $g' = g\Delta\rho/\rho_2$ is the reduced gravity (with $\Delta\rho = \rho_2 - \rho_1$ and ρ_k the kth layer density).

Finally, $\vec{T^w} = T_y^w \vec{j}$ represents the wind-driven acceleration which only applies in the first layer. Without loss of generality, it is chosen parallel to the y-axis and it can be expressed as (see for instance Bleck and Smith (1990), Cushman-Roisin (1994)):

$$T_y^w = \frac{\tau_o}{\rho_1\, h_1}, \tag{3}$$

where τ_o is the wind stress at the surface and will be considered constant in this study: $\tau_o = 0.5\ \mathrm{N/m^2}$. T_y^w can, however, vary if h_1, the first layer thickness, varies. In the following, some experiments will be carried out where T_y^w will be artificially forced to remain constant by replacing h_1 by H_1, the first (upper) layer thickness at rest.

In the following, Eqs. (1) and (2) will be solved numerically using a version of the Miami Isopycnal Coordinate Ocean Model (MICOM; see Bleck and Boudra (1986), Bleck and Smith (1990), Bleck et al. (1992)) described in Herbette et al. (2003), Morel et al. (2006) and Winther et al. (2007).

2.2. Ekman drift

If τ_o is spatially constant and if the ocean is initially at rest with constant layer depths $h_k = H_k$ at $t = 0$, then the solution of Eqs. (1) and (2) is given by:

$$U_1 = \frac{\tau_o}{f\rho_1 H_1}(1 - cos(ft)),$$
$$V_1 = \frac{\tau_o}{f\rho_1 H_1} sin(ft),$$
$$(U_2, V_2) = (0, 0),$$
$$h_k = H_k. \tag{4}$$

Notice that in the first layer, there exists a mean displacement of fluid parcels perpendicular to the direction of the wind, the Ekman drift. Its strength is given by (see Ekman (1905), Pedlosky (1987), Cushman-Roisin (1994)):

$$U_{Ek} = \frac{\tau_o}{f\rho_1 H_1}. \tag{5}$$

In this study, we will consider a constant northward wind stress $\tau_o = 0.5\ \mathrm{N/m^2}$ which will be applied at $t = 0$ and its effect on the propagation of vortices evaluated. Unless stated otherwise the duration of the simulations will be 100 days. Notice that for $H_1 = 500$ m (chosen for most of the study, see below), the Ekman drift speed in the first layer is:

$$U_{\mathrm{Ek}} \simeq 1\mathrm{cm/s}, \tag{6}$$

so that the displacement of water parcels subject to this drift for 100 days is about $L_{Ek}^{100} \simeq 86.4$ km.

2.3. Potential vorticity

Potential vorticity (PV) is defined by:

$$PV = \frac{\zeta + f}{h}, \tag{7}$$

where $\zeta = rot(\vec{U}) = \partial_x V - \partial_y U$ is the curl of the velocity field. As in Morel and McWilliams (2001), Herbette et al. (2003), Morel et al. (2006), we define the PV anomaly (PVA) by

$$\begin{aligned}\Delta Q &= H * (PV - PV^{ref}) \\ &= H * \left(\frac{\zeta + f}{h} - \frac{f}{H}\right) \\ &= \frac{H}{h}\left(\zeta - f\frac{\Delta h}{H}\right), \end{aligned} \tag{8}$$

where $H = h_{\text{rest}}$ is the layer thickness of the fluid at rest, and $\Delta h = h - H$. Here, ΔQ has the same properties of Lagrangian conservation as PV, but it is directly related to the quasigeostrophic PV, has the dimension of a vorticity and its value at rest is zero, which makes it easier to analyse.

Indeed, under the hypothesis of geostrophic equilibrium, the PVA can be inverted to calculate the associated velocity field. As shown in Hoskins et al. (1985) (see also Morel and McWilliams (2001) or Herbette et al. (2005) and references therein) a positive PVA pole is associated with a cyclonic horizontal circulation. The circulation is more intense in the core of the PVA and gradually decreases away from this core (see Fig. 1a and b). If the PVA pole is negative, the circulation is anticyclonic.

Dipolar structures are associations of two opposite sign PVA cores. Dipolar structures are known to have self propagation properties, the direction of propagation being driven by the position of the two PVA cores. Fig. 1c and d describes some configurations of interest for the following analysis.

If for instance the positive core is located on the western side of the negative one (Fig. 1c) then the dipole propagates southward. Notice this corresponds to a PVA structure of the form $q = F(r)\ x = F(r)\ r\ cos\theta$, where $F(r) \rangle 0$ and (r, θ) are polar coordinates.

If the positive core is located on the northern side of the negative one (Fig. 1d) then the dipole propagates westward. Notice this corresponds to a PVA structure of the form $q = F(r)\ y = G(r)\ r\ sin\theta$, where $G(r) \rangle 0$.

2.4. Initial vortex structure

To avoid boundary problems, in this paper we consider isolated vortices whose far-field velocities decrease more rapidly than $1/r$, where r is the distance from their center. Morel and McWilliams (1997) have shown that the integral of PVA is null for isolated vortices so that there must exist equal positive and negative PVA. Morel and McWilliams (1997) have then identified two main types of isolated vortices having different stability and propagation properties: S-vortices, when the opposite sign PVA are vertically aligned, R-vortices when the PVA are located in the same layers, with a core surrounded by an opposite sign PVA crown. While the former is unstable and forms hetonic structures (see Morel and McWilliams (1997)) with enhanced self propagation properties, the latter is generally more stable.

To avoid complication of the analysis due to instabilities or strong self propagation properties, we will concentrate on R-vortices with PVA structures of the type (see Carton and McWilliams (1989)):

$$\Delta Q_k = \Delta Q_k^o e^{-(r/R)^\alpha}\left(1 - \frac{\alpha}{2}(r/R)^\alpha\right), \tag{9}$$

where R is the radius of the vortex, ΔQ_k^o the strength of the PVA in layer k and α a stability parameter. Carton and McWilliams (1989) has shown that choosing $\alpha \leqslant 1.8$ yields stable structures for quasigeostrophic barotropic vortices. Our experience is that this is still the case for baroclinic structures with the same PVA structure, but vertically localized, provided ΔQ_k^o has the same sign for all layers.

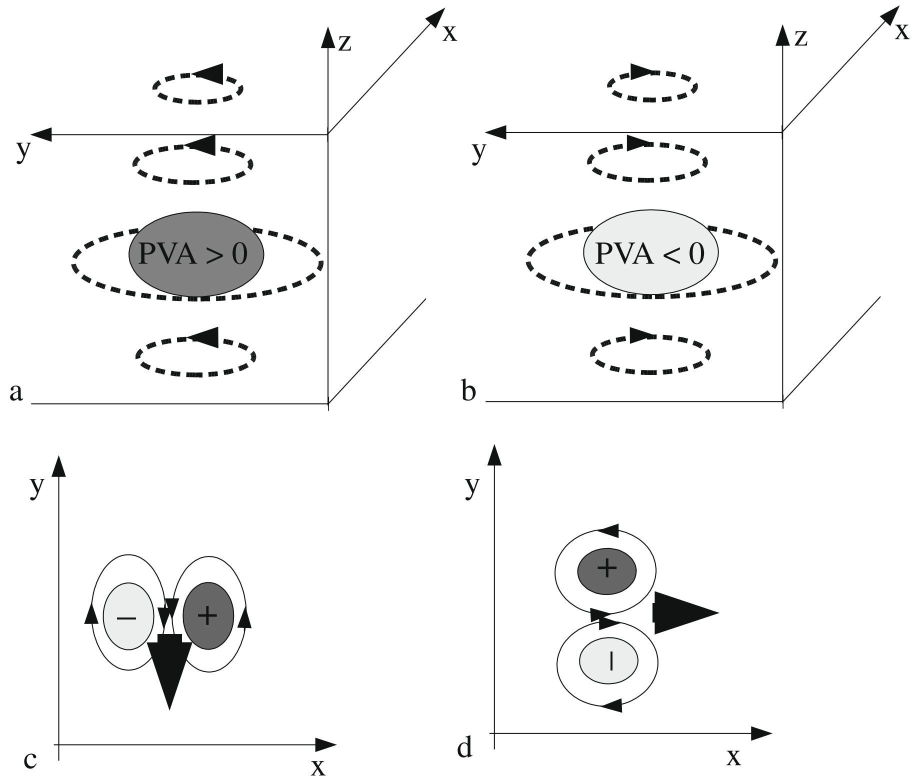

Fig. 1. Schematic of the PVA inversion principle. A positive PVA core is associated with a cyclonic circulation over the entire water column (a). A negative PVA core is associated with an anticyclonic circulation over the entire water column (b). A dipole is an association of opposite sign PVA cores and generates propagation (c and d).

In the following we will concentrate on two-layer configurations with variable vortex structure but with the same stability parameter: $\alpha = 1.5$.

Notice that to have null integrated PVA Eq. (9) above only gives an approximation of the PVA of the vortex and that an iterative procedure has to be used to determine an exact isolated structure (see Herbette et al. (2003)), however, the final structure is close to this approximation.

Once the vortex characteristics are chosen, Eq. (9) can be inverted under the assumption of cyclo-geostrophic equilibrium (see Herbette et al. (2003)) to calculate the initial layer thickness and velocity field.

2.5. Parameters

In this study, there are seven configuration parameters which can be varied: $R, \Delta Q_1^o, \Delta Q_2^o, H_1, H_2, \Delta\rho/\rho_2, \tau_o$ (note g, f and ρ_1 are additional configuration parameters but they are considered fixed). Nondimensionalising Eq. (1) also yields three additional non-dimensional parameters (the Rossby number, the Froude number and an Ekman number). Two (one vertical, one horizontal) length scales, one time scale and one density scale can be chosen to non-dimensionalise the problem, so that there "only" exists six independent parameters in this study. This is still by far too many and no exhaustive analysis can be undertaken. We will, therefore, base our study on a reference experiment and sensitivity studies for some parameters.

First, as mentioned above, the wind stress at the surface is kept constant with $\tau_o = 0.5$ N/m^2. In most of the study, the background stratification is also fixed with: $H_1 = H_2 = 500$ m and $\Delta\rho/\rho_2 = 1^o/_{oo}$. Notice this yields an internal radius of deformation $R_d = \sqrt{g' H_1 H_2/(H_1+H_2)}/f \simeq 15.6$ km. The three remaining parameters that can be varied are the vortex radius and PVA strengths ($R, \Delta Q_1, \Delta Q_2$, see Table 1).

Finally, for numerical experiments, the grid step of the numerical model, Δx, will be adapted so as to correctly resolve the vortex structure ($\Delta x = R/10$, where R is the vortex radius defined in 9) and the time steps will be chosen so as to avoid numerical instabilities.

3. Reference experiments

We first illustrate the complexity of the interaction of a vortical structure with the wind stress. Fig. 2 presents the upper layer depth and velocity fields in both layers for a surface intensified cyclonic vortex chosen for our reference experiments (experiments cst1 and var1 in Table 1). Its PVA structure is given by a radius $R = 40$ km and $\Delta Q_1 = 0.5f, \Delta Q_2 = 0$.

Table 1
Characteristics of all the experiments presented in the sensitivity studies. Notice that all experiments have been performed with the same stratification parameters defined above (in particular $H_1 = H_2 = 500$ m) except experiments var9 and var10, for which (H_1, H_2) = (100 m, 900 m) and (H_1, H_2) = (500 m, 1500 m), respectively.

Exp No.	T_y^w	Δx (in km)	R (in km)	$\Delta Q_1/f$	$\Delta Q_2/f$
cst1	$\tau_o/\rho_1 H_1$	4	40	0.5	0
var1	$\tau_o/\rho_1 h_1$	4	40	0.5	0
var2	$\tau_o/\rho_1 h_1$	4	40	0	0.5
var3	$\tau_o/\rho_1 h_1$	4	40	0.5	0.5
cst3	$\tau_o/\rho_1 H_1$	4	40	0.5	0.5
var4	$\tau_o/\rho_1 h_1$	4	40	−0.5	0
var5	$\tau_o/\rho_1 h_1$	4	40	1	0
var6	$\tau_o/\rho_1 h_1$	4	40	0.25	0
var7	$\tau_o/\rho_1 h_1$	8	80	0.5	0
var8	$\tau_o/\rho_1 h_1$	2	20	0.5	0
var9	$\tau_o/\rho_1 h_1$	4	40	0.5	0
var10	$\tau_o/\rho_1 h_1$	4	40	0.5	0

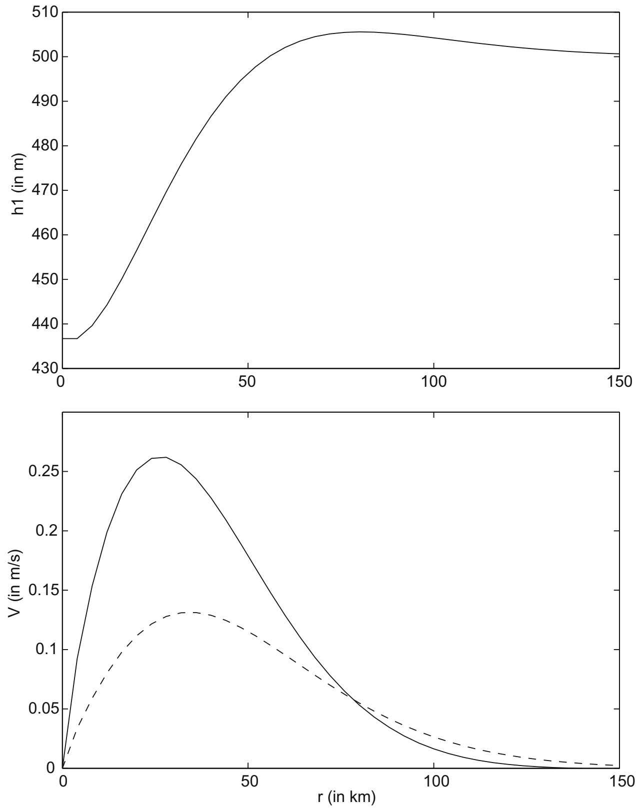

Fig. 2. Upper panel: first layer thickness h_1 at $t = 0$ as a function of the distance from the vortex center (r). Lower panel: first (plain line) and second (dashed line) layer azimuthal velocity field V_θ at $t = 0$ as a function of the distance from the vortex center (r).

Notice the velocity field is positive (cyclonic rotation), its maximum is about $V_{max} \simeq 0.26$ m/s and is reached at a distance $r \simeq 27$ km from the vortex center. The upper layer thickness diminishes near the vortex center, which is also consistent with a cyclonic vortex intensified in the upper layer.

As there is no background PVA associated with Ekman currents, the compensation mechanism described in Vandermeirsch et al. (2001) does not apply and we could imagine that Hogg and Stommel (1990) theory readily applies here. In the present case, as the vortex PVA is null in the second layer, if the wind-driven acceleration T_y^w is considered constant (h_1 is replaced by H_1 in Eq. (3) an apparent good approximation according to Fig. 2, upper panel), the exact solution of Eq. (1) is a mere superposition of the Ekman current and vortex structure (vortex velocity in cyclo-geostrophic equilibrium) drifting at the Ekman drift speed.[1] Fig. 3 shows the initial and final vortex PVA structure in the first layer, and the vortex trajectory in this case. The vortex indeed propagates eastward, to the right of the wind, and the total displacement for 100 days is 90 km, close to the expected 86.4 km (error less than a grid step, $\Delta x = 4$ km here).

Fig. 4 shows the same plot as in Fig. 3 but for an experiment where the variations of T_y^w with h_1 have been retained. The total eastward displacement is now drastically reduced (only 44 km, less than half the previous one). Notice that a crude analysis where the Ekman drift speed would be calculated using an average of h_1 over the vortex core would have yielded an increase of the "eastward" (the direction of the wind being assimilated as North) speed as $h_1 \leqslant H_1$ for the cyclonic vortex considered here. Notice that there now also exist a northward (along-wind) displacement of 12 km.

[1] Notice the fact that the PVA is null in layer two is necessary to get an exact solution propagating at Ekman drift speed. Also notice the velocity field is not zero in this case.

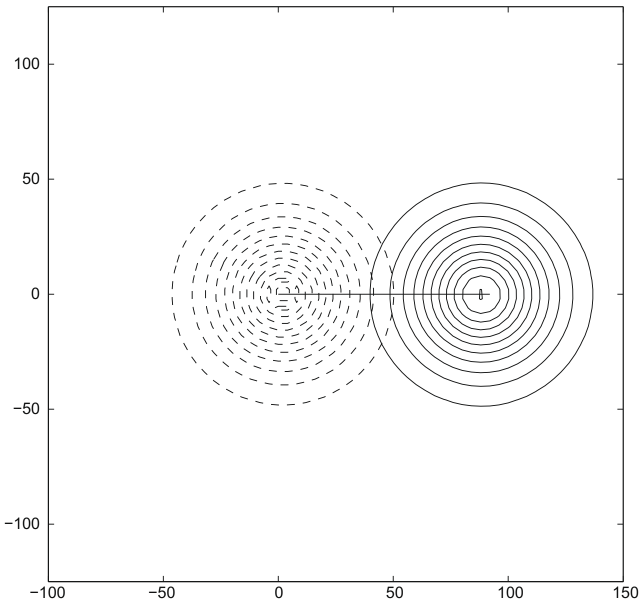

Fig. 3. Initial (dashed contours) and final (plain contours) PVA in layer 1 together with the vortex trajectory for a vortex structure $\Delta Q_1^o = 0.5f, \Delta Q_2^o = 0, R = 40km$ and with a constant wind-driven acceleration. Contours are every $0.05f$.

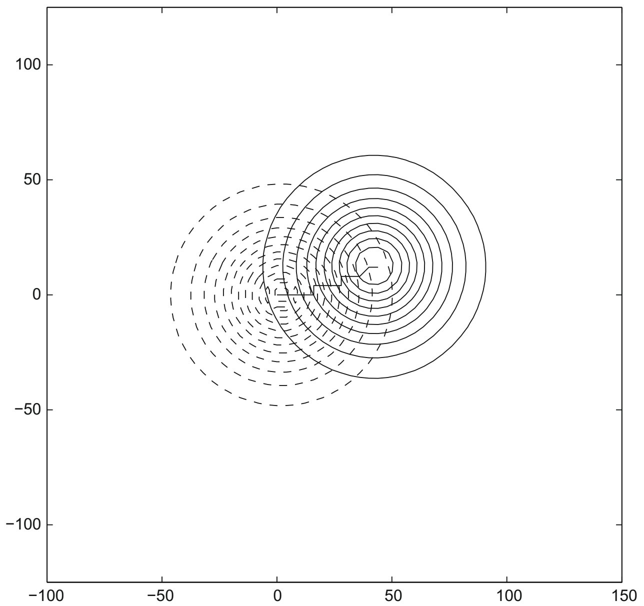

Fig. 4. Initial (dashed contours) and final (plain contours) PVA in layer 1 together with the vortex trajectory for a vortex structure $\Delta Q_1^o = 0.5f, \Delta Q_2^o = 0, R = 40km$ and with a wind-driven acceleration that varies with layer thickness. Contours are every $0.05f$.

4. Theoretical analysis

4.1. PV evolution equation

As shown in Morel et al. (2006), the PVA evolution equation in each layer is:

$$\frac{d\Delta Q_k}{dt} = \frac{H_k}{h_k} rot(\vec{T}_k^w). \tag{10}$$

As the wind-driven acceleration only applies in the first layer here, the PVA is conserved for each particles in the second layer:

$$\frac{d\Delta Q_2}{dt} = 0, \tag{11}$$

whereas for the first layer the PVA evolution can be written:

$$\frac{d\Delta Q_1}{dt} = \frac{H_1}{h_1}\partial_x T_y^w = -\frac{H_1 \tau_o}{\rho_1 h_1^3}\partial_x h_1. \tag{12}$$

Thus, as already noticed in Morel et al. (2006), a constant wind is able to generate potential vorticity anomalies, provided the upper layer thickness is not constant.[2]

4.2. Simplified equation

Notice that the source term in Eq. (12) resembles the classical Ekman pumping. However, as noticed above, it is not associated with the wind curl, but with the curl of the wind-driven acceleration along isopycnal surfaces when the vertical position of the latter varies. As for the classical Ekman pumping, Eq. (1) can be simplified considering the Rossby number is small: we only retain the Coriolis and Pressure gradient terms for geostrophic equilibrium and the wind-driven acceleration term. If we also consider $\Delta h_k \ll H_k$, we get the following simplified equations:

$$\begin{aligned} fV_k &\simeq \partial_x M_k \\ f(U_k - U_{Ek}\delta_{k,1}) &\simeq -\partial_y M_k \\ \frac{d\Delta Q_k}{dt} &\simeq -\frac{\tau_o}{\rho_1 H_1^2}\partial_x h_1 \delta_{k,1}. \end{aligned} \tag{13}$$

Eq. (13) can then be entirely written as a function of the streamfunction $\psi_k = M_k/f$, noticing that:

$$\begin{aligned} \Delta Q_k &\simeq \zeta_k - f\frac{\Delta h_k}{H_k}, \\ &\simeq \nabla^2\psi_k - f\frac{\Delta h_k}{H_k}, \end{aligned} \tag{14}$$

where $\nabla^2\psi = \partial_{xx}\psi + \partial_{yy}\psi$ is the Laplace operator.

For a flat bottom, neglecting the free surface elevation (rigid lid approximation) and using Eqs. (2) and (13) also yields:

$$\begin{aligned} \Delta h_1 &\simeq -\Delta h_2, \\ &\simeq f/g'(\psi_1 - \psi_2), \end{aligned} \tag{15}$$

and

$$\begin{aligned} \frac{d\Delta Q_k}{dt} &\simeq \partial_t \Delta Q_k + U_k\partial_x\Delta Q_k + V_k\partial_y \Delta Q_k, \\ &\simeq \partial_t\Delta Q_k + J(\psi_k - \delta_{k,1}U_{Ek}y, \Delta Q_k), \end{aligned} \tag{16}$$

with $J(A,B) = \partial_x A\partial_y B - \partial_y A\partial_x B$, the Jacobian operator.

We then end up with generalised quasigeostrophic equations for a two-layer configuration with additional terms coming from the wind stress in the first layer:

$$\begin{aligned} \partial_t\Delta Q_1 + J(\psi_1 - U_{Ek}y, \Delta Q_1) &\simeq -\frac{f\tau_o}{g'\rho_1 H_1^2}\partial_x(\psi_1 - \psi_2), \\ \partial_t \Delta Q_2 + J(\psi_2, \Delta Q_2) &\simeq 0. \end{aligned} \tag{17}$$

with

$$\begin{aligned} \Delta Q_1 &\simeq \nabla^2\psi_1 - F_1(\psi_1 - \psi_2), \\ \Delta Q_2 &\simeq \nabla^2\psi_2 - F_2(\psi_2 - \psi_1), \end{aligned} \tag{18}$$

[2] Notice that this is associated with the two-layer configuration considered here. For a more general – continuous – configuration, the correct explanation is that isopycnic levels can penetrate or leave depths where the wind stress extends, so that, even though the wind is constant, there can exist variations of wind-driven acceleration along isopycnic levels, which gives rise to stress torque and is a PVA source.

where

$$F_1 = \frac{f^2}{g'H_1},$$
$$F_2 = \frac{f^2}{g'H_2}. \tag{19}$$

Notice that the PVA source term, $-\frac{f\tau_o}{g'\rho_1 H_1^2}\partial_x(\psi_1 - \psi_2)$, can be interpreted as a sort of beta-effect in the upper layer and is null for purely barotropic dynamics (for which $\psi_1 - \psi_2 = \Delta h_1 = 0$). We thus define:

$$\hat{\beta} = \frac{f\tau_o}{g'\rho_1 H_1^2}. \tag{20}$$

For the parameters chosen here we find $\hat{\beta} \simeq 2 \times 10^{-11}\,\mathrm{s}^{-1}\,\mathrm{m}^{-1}$, which is comparable to the planetary beta coefficient at mid-latitude.

4.3. Linear wave dynamics

The propagation speed of vorticity waves subject to the effect of a wind stress can then be calculated, neglecting the nonlinear Jacobian operator in Eq. (17). Looking for solutions of the form:

$$\psi_k(x, y, t) = \Psi_k^o e^{i(kx+ly-\omega t)}, \tag{21}$$

we find that the dispersion equation for the propagation speed of the waves is:

$$\frac{\omega}{k} = C = U_{Ek} - U_{Ek}\frac{F_1}{F_1 + F_2 + k^2 + l^2} = U_{Ek}\frac{F_2 + k^2 + l^2}{F_1 + F_2 + k^2 + l^2}. \tag{22}$$

The propagating mode is associated with a wave whose vertical structure is given by $\Psi_2 = \frac{F_2}{F_2+k^2+l^2}\Psi_1$. There also exists a non-propagating mode associated with a structure where the upper layer is at rest $\Psi_1 = 0$.

The propagation speed is always smaller than the Ekman drift. For short waves (wavelength much smaller than the internal radius of deformation), we simply recover the Ekman drift: $C = U_{Ek}$; but for long waves (wavelength much larger than the internal radius of deformation), we find:

$$C = U_{Ek}\frac{F_2}{F_1 + F_2},$$
$$= U_{Ek}\frac{H_1}{H_1 + H_2}, \tag{23}$$

The PVA source term can thus drastically reduce the propagation speed of waves as soon as their wavelength is comparable to, or larger than, the internal radius of deformation.

4.4. Comparison between Stern and the present results

All the previous equations were already derived in Stern (1965). Indeed, as mentioned above, Stern (1965) derived a generalised quasigeostrophic equation that takes into account the non-linear interactions between a geostrophic vortex and a uniform wind stress. Stern considered a wind-driven turbulent stress confined to a thin frictional layer on top of a homogeneous mixed layer. He showed that Ekman pumping is generated by a uniform wind at the top of the mixed layer when a pre-existing vortex is considered. Stern then derived the vorticity equation of the geostrophic part of the motion in the mixed layer and showed that Ekman pumping leads to vortex stretching/squashing driving in turn the vortex propagation. Finally, Stern calculated the dispersion relation associated with this effect in a two-layer model and showed that long waves propagate at a speed smaller than the Ekman drift.

In the present paper we study the same process (propagation of a pre-existing vortex associated with a uniform wind) with the same configuration (two-layer model), but a different parameterization is considered for the wind-driven acceleration: the wind stress is uniformly distributed over the depth of the homogeneous upper layer. Variations of the upper layer thickness then induces variations of wind-driven acceleration. This modifies the PVA evolution and an additional horizontal circulation is generated over the vortex core area which disturbs the advection of fluid parcel by the Ekman drift (see next section).

There thus apparently exists important differences between Stern (1965) and the present study in the parameterization of the wind-driven acceleration and analysis of its effect on the vortex displacement. It is then striking to see that both approaches yield identical results: Eq. (17) (for layer 1) is indeed the same[3] as Stern's new equation (Eq. (6) in his paper) and the propagation speed of linear waves are identical in both studies (some manipulations of Eq. (22) indeed yield Stern's Eq. (24)). This shows that, despite the differences in the parameterization of the wind-driven acceleration, the effects studied in Stern (1965) and here are identical, and the following developments propose some complementary analysis for the process discovered by Stern.

Notice the previous linearized calculations are not valid for strong (coherent) cyclo-geostrophic vortices for which particular behavior can also be expected. For instance, the along-wind displacement observed in the reference experiment can not be explained and was not predicted in Stern (1965). We therefore, now propose new calculations to take the vortex coherency into account.

4.5. Beta-gyre for vortices

Notice that neglecting the wind-driven acceleration variations is equivalent to neglecting the source term on the right hand side of the first layer PVA evolution Eq. (17). In this case we recover the usual quasigeostrophic equations used for instance in Hogg and Stommel (1990), and all their results apply. As shown in Hogg and Stommel (1990) the maintenance of the vortex vertical coherency has some impact on its propagation speed, which is no longer given by the upper layer (Ekman) drift speed but is an average of the background velocity weighted by the vortex vertical PVA structure. If ΔQ_1^o and ΔQ_2^o are the PVA strength in layers 1 and 2, the propagation speed of the vortex is typically given by:[4]

$$U_{hs90} \simeq \frac{H_1 U_{Ek}\Delta Q_1^o}{H_1\Delta Q_1^o + H_2\Delta Q_2^o}. \tag{24}$$

Let us now analyse the influence of the wind stress term. In the reference frame moving with the vortex, the vortex mainly keeps its initial axisymmetric structure. The PVA evolution in the first layer is then:

$$\frac{d\Delta Q_1}{dt} = -\frac{H_1\tau_o}{\rho_1\bar{h}_1^3}\partial_r\bar{h}_1 cos\theta, \tag{25}$$

where r is the distance from the vortex center, θ the angle relative to the x-axis, $\bar{h}_1$ the initial axisymmetric upper layer thickness and $\partial_r\bar{h}_1$ its radial derivative.

Thus, at first order, a vortex generates dipolar PVA when it interacts with a wind stress. This dipolar PVA is itself associated with a current, similar to the beta-gyre studied in Sutyrin and Flierl (1994), Sutyrin and Morel (1997) or Vandermeirsch et al. (2001),

[3] Taking into account the geostrophic assumption and grouping the $U_{Ek}.\vec{\nabla}Q_1$ term with the PVA source term, $-\frac{f\tau_o}{g'\rho_1 H_1^2}\partial_x(\psi_1 - \psi_2)$.

[4] The Hogg and Stommel (1990) analysis is based on a two-layer reduced gravity configuration and with point vortices, but in practice their results roughly apply to extended vortices, provided the PVA structure remains axisymmetric in each layer.

that in turn induces vortex propagation. For instance Eq. (25) shows that an upper layer cyclonic vortex, for which $\partial_r \bar{h}_1 \geqslant 0$ over the vortex core, generates a negative potential vorticity anomaly on the side of the vortex to the right of the wind, and a positive potential vorticity anomaly on the side of the vortex at the left of the wind. This induces a mean current, and a displacement of the vortex, along the wind, northward in the present case. This is exactly what is observed in the reference experiment presented above. For an upper layer anticyclonic vortex, the dipole would be inverted as $\partial_r \bar{h}_1 \leqslant 0$ over the vortex core, and we expect a southward displacement. In addition to the Ekman drift perpendicular to the wind, we can thus expect displacements parallel to the wind for vortices.

Taking advantage of the resemblance of Eqs. (17) and (18) with the well studied QG equation for the influence of the planetary beta effect on vortices, we can find some theoretical ground to further analyse the influence of the wind stress term. Indeed, following Vandermeirsch et al. (2001) we can decompose the vortex propagation into three different components: advection by the background current (Hogg and Stommel (1990) result, roughly given by Eq. (24)), the development of a dipolar beta-gyre, here induced by the wind, and the influence of the vortex structure deformation (both horizontal and vertical) in particular induced by the beta-gyre development. As in Sutyrin and Flierl (1994), Sutyrin and Morel (1997) and Vandermeirsch et al. (2001), the beta-gyre is defined in the reference frame moving with the vortex (where the origin is given by the extremum of the streamfunction). In this reference frame, the streamfunction and potential vorticity keep their initial structure and remain axisymmetric at first order for coherent vortices. The evolutive terms responsible for the vortex propagation are anomalies that scale with the small parameter $\hat{\beta}R/\Delta Q_1^o$ (or $\hat{\beta}R/\Delta Q_2^o$ when $\Delta Q_1^o = 0$). The beta-gyre is then defined as the potential vorticity anomaly generated by the potential vorticity source term (the "beta-effect" term) and advected by the axisymmetric circulation. Its evolution equation is given at first order by (in polar (r,θ) coordinates):

$$\partial_t q_1 + J(\bar{\psi}_1, q_1) = -\frac{\tau_o}{\rho_1 H_1^2}\partial_r \bar{h}_1 cos\theta, \quad (26)$$

where q_1 is the PVA associated with the beta-gyre and $\bar{\psi}_1$ the initial upper layer axisymmetric streamfunction. Eq. (26) is linear and can be solved taking into account $q_1(r,\theta,t=0)=0$. The solution is:

$$q_1 = \frac{\tau_o \partial_r \bar{h}_1}{\rho_1 H_1^2 \overline{\Omega}_1}[sin(\theta - \overline{\Omega}_1 t) - sin\theta], \quad (27)$$

or

$$q_1 = \frac{\tau_o \partial_r \bar{h}_1}{\rho_1 H_1^2 \overline{\Omega}_1}[sin(\theta)cos(\overline{\Omega}_1 t) - cos(\theta)sin(\overline{\Omega}_1 t) - sin\theta], \quad (28)$$

where $\overline{\Omega}_1 = \partial_r \bar{\psi}_1 / r$ is the rotation rate in the upper layer.

The dipolar velocity field, associated with q_1 and responsible for the additional vortex propagation, can then be calculated (see Sutyrin and Flierl (1994), Sutyrin and Morel (1997), Vandermeirsch et al. (2001)). The deformation of the vortex structure and its effect can, however, also strongly affect the vortex displacement. Note that a precise analytical model taking all effects into account could be developed following Sutyrin and Flierl (1994), Sutyrin and Morel (1997), Vandermeirsch et al. (2001) (this however, requires us to consider vortices with piecewise constant PVA structures). For the qualitative explanations we seek here, the effect of deformation will be neglected, and we will concentrate on the direct effect of the beta-gyre development alone, as given by Eqs. (27) or (28).

First notice that, as described in Section 2.3, the along-wind displacement is associated with the $cos\theta$ term whereas the cross wind displacement is associated with the $sin\theta$ term. Also, the along wind displacement is positive (in the direction of the wind) when the coefficient of the $cos\theta$ term is negative. The cross wind displacement is positive (to the right of the wind) when the coefficient of the $sin\theta$ term is positive.

Eq. (28) then shows that the initial displacement is oriented along the wind and its sign depends on the sign of $-\partial_r \bar{h}_1$ as already noticed above. Four cases can be distinguished:

(1) In the case of a cyclonic vortex intensified in the upper layer, $-\partial_r \bar{h}_1$ is negative and the along wind displacement is in the direction of the wind.
(2) In the case of an anticyclonic vortex intensified in the upper layer, $-\partial_r \bar{h}_1$ is positive and the along wind displacement is opposed to the direction of the wind.
(3) In the case of a cyclonic vortex intensified in the lower layer, $-\partial_r \bar{h}_1$ is positive and the along wind displacement is opposed to the direction of the wind.
(4) In the case of an anticyclonic vortex intensified in the lower layer, $-\partial_r \bar{h}_1$ is negative and the along wind displacement is in the direction of the wind.

The cross wind displacement associated with the beta-gyre can be evaluated asymptotically, noticing, as in Sutyrin and Flierl (1994), Sutyrin and Morel (1997), Vandermeirsch et al. (2001), that the time dependent term contribution tends toward zero because of the differential rotation rate which homogenizes the beta-gyre (opposite sign filaments are rolled up into a spiral that have weak integrated effect) so that the structure tends toward

$$q_1 = -\frac{\tau_o \partial_r \bar{h}_1}{\rho_1 H_1^2 \overline{\Omega}_1} sin\theta, \quad (29)$$

whose sign depends on the sign of $-\partial_r \bar{h}_1 / \overline{\Omega}_1$. Again, the four previous cases can be distinguished:

(1) In the case of a cyclonic vortex intensified in the upper layer, $-\partial_r \bar{h}_1 / \overline{\Omega}_1$ is negative and the cross wind displacement associated with the beta-gyre is at the left of the wind, compensating the Ekman drift. This is indeed what is observed for the reference experiment.
(2) In the case of an anticyclonic vortex intensified in the upper layer, $-\partial_r \bar{h}_1 / \overline{\Omega}_1$ is also negative, again leading to a compensation of the Ekman drift.
(3) In the case of a cyclonic vortex intensified in the lower layer, $-\partial_r \bar{h}_1 / \overline{\Omega}_1$ is positive, which yields a propagation to the right of the wind reinforcing the Ekman drift (normally playing no advection role in the lower layer).
(4) In the case of an anticyclonic vortex intensified in the lower layer, $-\partial_r \bar{h}_1 / \overline{\Omega}_1$ is positive, yielding again a propagation to the right of the wind reinforcing the Ekman drift (normally playing no advection role in the lower layer).

Finally, notice that the beta-gyre can also be written:

$$\begin{aligned} q_1 &= \frac{f\tau_o}{\rho_1 g' H_1^2}\frac{\partial_r(\bar{\psi}_1 - \bar{\psi}_2)}{\partial_r \bar{\psi}_1} r[sin(\theta - \overline{\Omega}_1 t) - sin\theta], \\ &= \frac{f\tau_o}{\rho_1 g' H_1^2}\frac{\overline{V}_1 - \overline{V}_2}{\overline{V}_1} r[sin(\theta - \overline{\Omega}_1 t) - sin\theta], \\ &= \frac{f\tau_o}{\rho_1 g' H_1^2}\frac{\overline{\Omega}_1 - \overline{\Omega}_2}{\overline{\Omega}_1} r[sin(\theta - \overline{\Omega}_1 t) - sin\theta], \end{aligned} \quad (30)$$

where $\overline{V}_k$ is the azimuthal velocity in layer k and $\overline{\Omega}_k = \overline{V}_k / r$ is the rotation rate.

Thus, the upper layer stratification characteristics, but also any parameter possibly modifying the vertical structure of the vortex velocity, can have an influence on the strength of the beta-gyre, and associated additional displacement, which is complex and justifies the following sensitivity study.

5. Qualitative validation and sensitivity studies

In this section we study the sensitivity of the beta-gyre to several parameters associated with the vortex structure and the background stratification. Table 1 provides a recapitulation of all the experiments presented in the following with their characteristics.

5.1. Influence of the vortex vertical structure

To validate the theoretical results of the previous sections, we first evaluate the influence of the vortex vertical structure, and consider a vortex intensified in the lower layer with $\Delta Q_1^o = 0, \Delta Q_2^o = 0.5f$ (experiment "var2" in Table 1). As expected from the previous theoretical analysis, Fig. 5, which now represents the initial and final PVA and vortex trajectory in the lower layer, shows that the cross wind trajectory is to the right of the wind, and the along wind displacement against the wind. This is qualitatively consistent with the beta-gyre theory developed above.

Notice in this case that U_{hs90} is null (there is no mean current in the layer of the vortex core) so that the observed vortex displacement is entirely due to the beta-gyre development (when this effect is neglected, the vortex does not move. This has been checked using an artificially constant wind-driven acceleration, again replacing h_1 by H_1 in 3). The total longitudinal displacement is ΔX = 52 km, slightly above the reference experiment, showing that subsurface vortices can be advected very efficiently and as much as surface vortices. In fact two effects compensate in this case: the beta-gyre develops in the upper layer and thus has weaker advective effects in subsurface layers, but the strength of the beta-gyre is increased for subsurface vortices as it is inversely proportional to Ω_1, which is weaker in this case (see Eq. (27)).

In the present configuration, the beta-gyre can be easily identified, and the quantitative analysis can be pushed further. Fig. 6 indeed represents the final PVA (t = 100 days) in the upper layer (note it is initially null, if it was not for weak numerical artifacts) whose structure is mainly dipolar. Spiraling associated with the entrainment of the generated PVA by the vortex cyclonic circulation is also obvious. Notice that the maximum generated PVA reaches about 0.013f which is pretty weak, but enough to generate a background advective current of $\simeq$ 0.5 cm/s. Also notice the small scale extrema of PVA in the vortex core, near the center. This pole is actually present at the beginning of the experiment and is advected later on. It is due to numerical errors close to the vortex center in the inversion problem for the initial structure, and that we have not been able to suppress. Notice it is very small (maximum 0.003f) in comparison with ΔQ_o and it plays no significant role in the process studied here.

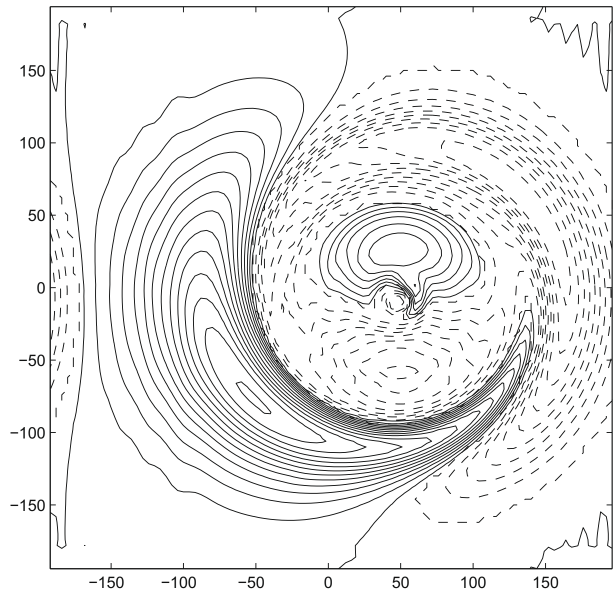

Fig. 6. Final PVA in layer 1 for a vortex structure $\Delta Q_1^o = 0, \Delta Q_2^o = 0.5f, R = 40km$. Contours are every 0.001f, dashed for negative PVA, plain for positive PVA. Notice the development of the beta-gyre associated with the wind stress.

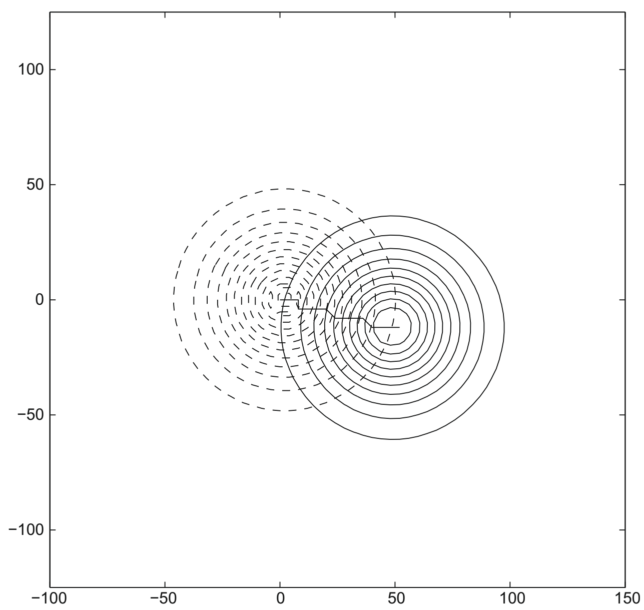

Fig. 5. Initial and final PVA in layer 2 together with the vortex trajectory for a vortex structure $\Delta Q_1^o = 0, \Delta Q_2^o = 0.5f, R = 40$ km.

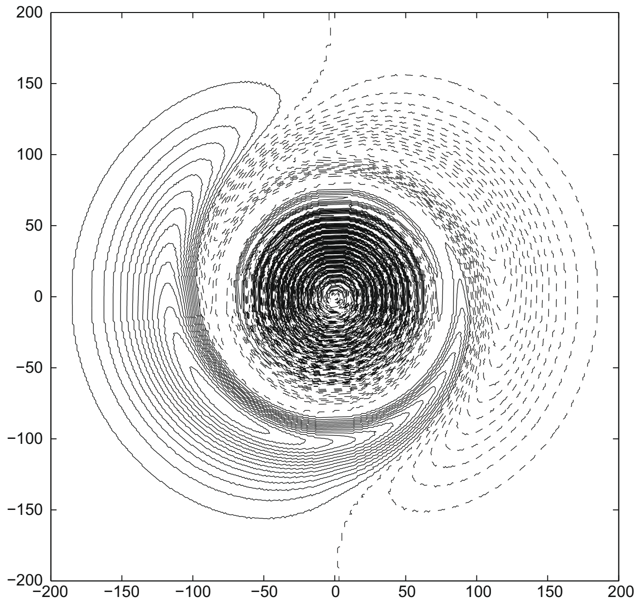

Fig. 7. Final (after 100 days) PVA in layer 1 calculated from Eq. (27) for a vortex structure $\Delta Q_1^o = 0, \Delta Q_2^o = 0.5f, R = 40km$. Contours are every 0.001f, dashed for negative PVA, plain for positive PVA. Notice the development of the strong spiraling in the vortex core.

Fig. 7 represents the beta-gyre for the same vortex structure but calculated using Eq. (27) (at time $t = 100$ days). Notice the similarities with Fig. 6, in particular, the maximum PVA reaches about $0.015f$ here. Also notice the strong variability in the core of the vortex, with opposite sign PVA filaments rolled up into a spiral by the differential vortex rotation. This spiraling structure has weak effects on the velocity field. Indeed, the latter is obtained by inverting the PVA field and the opposite sign filaments have balancing contributions (the structure of the relative vorticity field is similar to the PVA one for small scale structures and as the velocity is obtained by integrating the vorticity, opposite sign filaments balance). To have the PVA tendency in the vortex core, we can smooth the analytical structure. Fig. 8 is the result of such a smoothing and the PVA structure is now quite close to the numerical one, for which diffusion and viscosity act so as to eradicate small scale PVA structures. Notice the development of a dipolar structure in the vortex core, associated with Eq. (29).

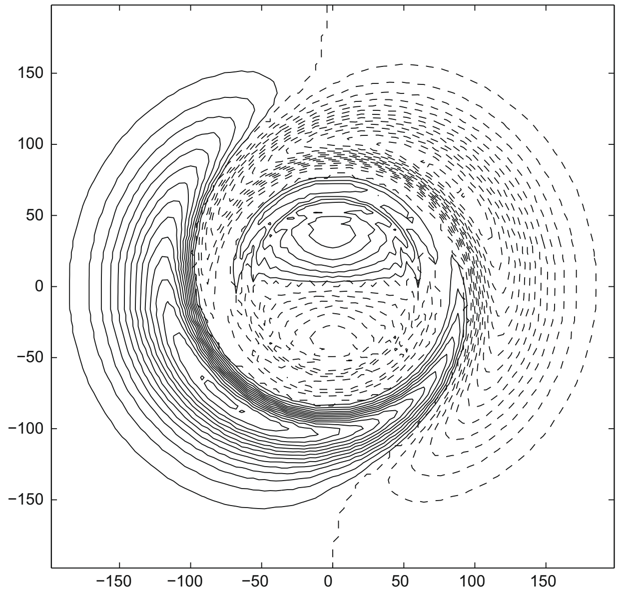

Fig. 8. Same as Fig. 7 except the PVA field has been smoothed so that the spiraling in the vortex core has been damped.

Fig. 9 represents a more detailed comparison between the numerical and analytical (from the smoothed solution) PVA solutions: here, we have plotted North–South PVA profiles across the vortex core to compare the strength of the dipolar structure that emerges in the vortex core. Notice the similarities, apart from the small artifact in the numerical solutions, associated with the initial PVA errors, and from the noise of the analytical solution associated with the remaining spiral structure. In particular, the mean PVA gradient is pretty similar and is about $\overline{\partial_y q_1} \simeq 1.810^{-11} s^{-1}.m^{-1}$ comparable to the planetary beta.

All these results validate our calculations and hypothesis.

Another easy way to validate our analysis is to consider a barotropic vortex for which $\Delta Q_1^o = \Delta Q_2^o$. Indeed, in this case h_1 or $V_1 - V_2 = 0$ so that no beta-gyre should develop. In fact as the vortex is subject to a vertically sheared background current, it will be deformed and tilted, developing a baroclinic component, which can then be associated with beta-gyre development. But the latter effect proves to remain modest: Figs. 10 and 11 represent the initial and final PVA in the upper layer together with the vortex trajectory for a barotropic structure ($\Delta Q_1^o = \Delta Q_2^o = 0.5f$, cases "var3" and "cst3" in Table 1). The two cases are identical, except that we have neglected the wind-driven acceleration variations for Fig. 11. Notice that the two plots are similar, underlining the absence of dipolar circulation or beta-gyre development, as expected. Also notice that the vortex drift associated with the Ekman current is smaller than for a vortex intensified in the upper layer as proved by Hogg and Stommel (1990) (about half in the present case with $H_1 = H_2$).

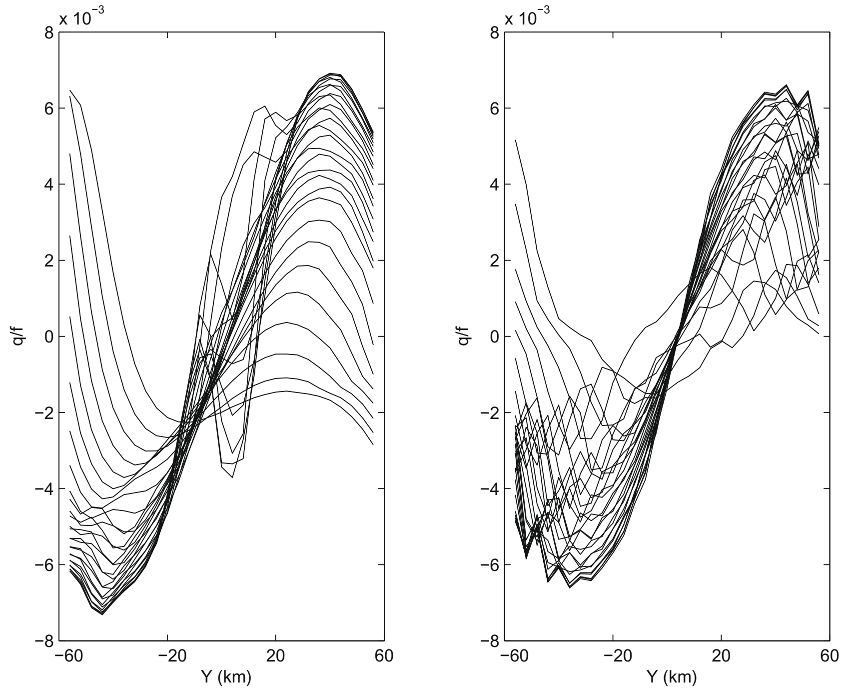

Fig. 9. Comparison of the beta-gyre structures (q/f) between the numerical (left) and analytical (right) calculations. to concentrate on the North–South dipolar component developing in the vortex core (see Fig. 8), q/f has been plotted as a function of y (with the origin taken at the vortex center), each line representing the profile at a fixed x position, near the vortex center ($x \in [-60, 60]km$). Notice the similarity of the mean North–South gradients for the numerical and analytical solutions.

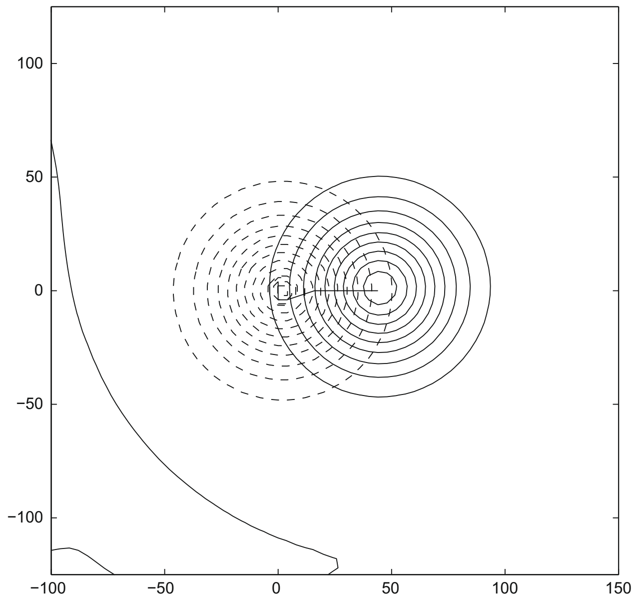

Fig. 10. Initial and final PVA in layer 1 together with the vortex trajectory for a barotropic vortex structure $\Delta Q_1^o = 0.5f, \Delta Q_2^o = 0.5f, R = 40$ km.

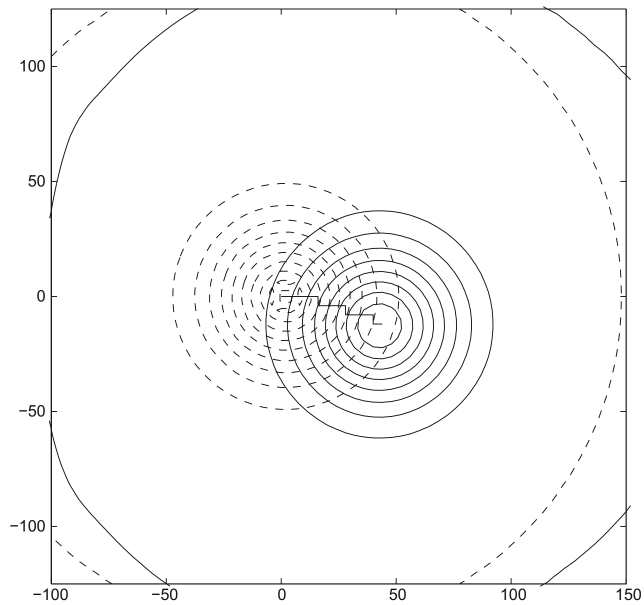

Fig. 12. Initial and final PVA in layer 1 together with the vortex trajectory for a vortex structure $\Delta Q_1^o = -0.5f, \Delta Q_2^o = 0, R = 40$ km.

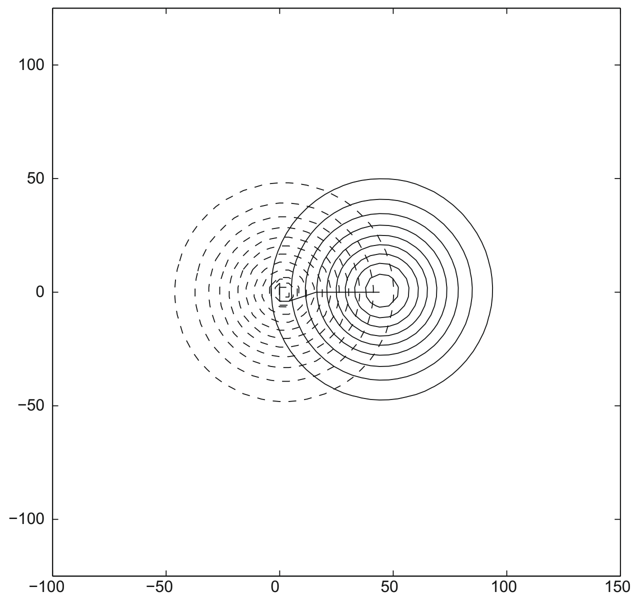

Fig. 11. Initial and final PVA in layer 1 together with the vortex trajectory for a barotropic vortex structure $\Delta Q_1^o = 0.5f, \Delta Q_2^o = 0.5f, R = 40$ km and with a constant wind-driven acceleration.

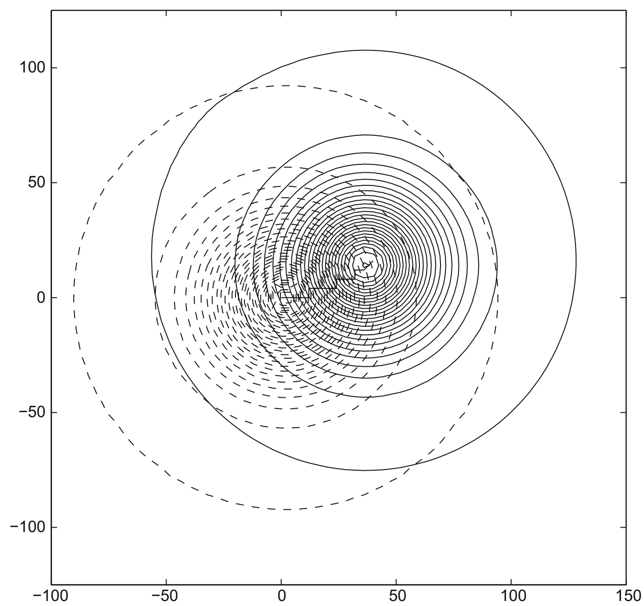

Fig. 13. Initial and final PVA in layer 1 together with the vortex trajectory for a vortex structure $\Delta Q_1^o = 1f, \Delta Q_2^o = 0, R = 40$ km.

5.2. Influence of the vortex sign

As another simple test to validate the theoretical results presented above, we also resume the reference experiment with exactly the same characteristics for the stratification, wind stress and vortex except for the sign of the latter: we here consider an anticyclonic vortex with $\Delta Q_1^o = -0.5f, \Delta Q_2^o = 0$ (experiment "var4" in Table 1). Fig. 12 represents the vortex initial and final PVA structure and the vortex trajectory. Notice the cross wind trajectory is identical to the cyclonic case, but the along wind displacement is now against the wind, as expected from the theoretical calculations. Also notice that the trajectory is almost the exact North–South symmetric of the reference experiment (see Fig. 4), which is also expected from the theory.

5.3. Influence of the vortex strength and radius

According to Eq. (30), the vortex structure can also play a role in the development of the beta-gyre we have identified. We can not perform an exhaustive sensitivity analysis in the present paper, and we have thus chosen to restrict our attention to the vortex size and strength. We have thus performed a few sensitivity studies varying the maximum PVA of the vortex, ΔQ_1^o, and its radius R (see Eq. (9)).

First, we have doubled ($\Delta Q_1^o = 1f$, Fig. 13) and reduced by half ($\Delta Q_1^o = 0.25f$, Fig. 14) the maximum PVA value with respect to the reference experiment (case "var5" and "var6" in Table 1). The trajectories are quite similar to the reference experiment (cross wind displacement 40 and 48 km, respectively, along wind dis-

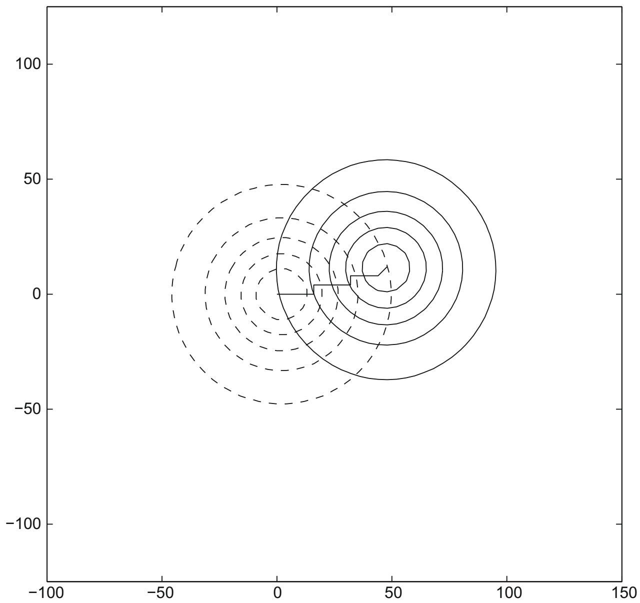

Fig. 14. Initial and final PVA in layer 1 together with the vortex trajectory for a vortex structure $\Delta Q_1^o = 0.25f, \Delta Q_2^o = 0, R = 40$ km.

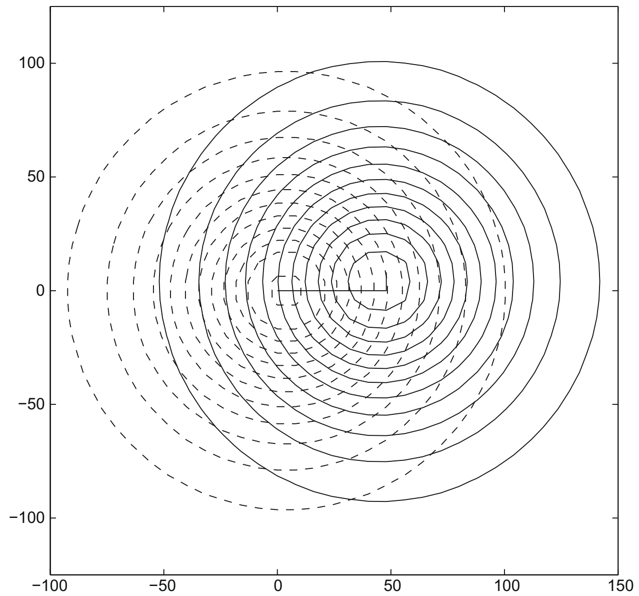

Fig. 15. Initial and final PVA in layer 1 together with the vortex trajectory for a vortex structure $\Delta Q_1^o = 0.5f, \Delta Q_2^o = 0, R = 80$ km.

placement 16 and 12 km) showing that the vortex strength only has a weak influence on the vortex trajectory at least for the present choice of configuration. This is, in fact, not surprising for the cross wind displacement as for the latter only the ratio $(V_1 - V_2)/V_1$ intervenes, which does not depend on ΔQ_1^o.

In Figs. 15 and 16 the vortex radius has been doubled (R = 80 km, Fig. 15, case "var7") and reduced by half (R = 20 km, Fig. 16, case "var7") with respect to the reference experiment. Again, the cross wind displacement has been only slightly modified ($\Delta X = 48$ and 50 km, respectively, for Figs. 15 and 16). The along wind displacement has however been strongly affected for the small (ΔY = 24 km: twice the displacement of the reference experiment) and the large vortex (ΔY = 8 km, hardly visible on the plot as it represents only one grid step in Fig. 15). This shows that, at

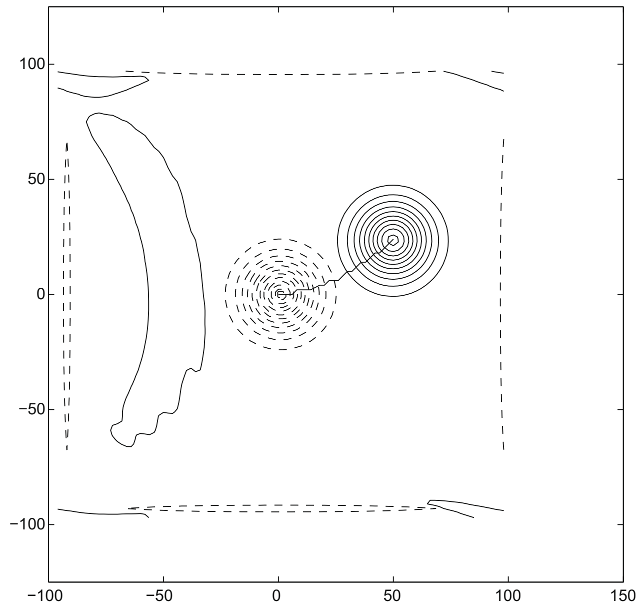

Fig. 16. Initial and final PVA in layer 1 together with the vortex trajectory for a vortex structure $\Delta Q_1^o = 0.5f, \Delta Q_2^o = 0, R = 20$ km.

least below some length scale, the along wind propagation depends on the vortex size and increases for small vortices.

The overall sensitivity of the trajectory to the vortex characteristics is, however, surprisingly weak. Eq. (30) indeed shows that the dependency of the beta-gyre on the vortex structure, and in particular its size, is not simple. As vortices propagating on the planetary beta-plane have a tendency to propagate at the speed of the long waves in some circumstances (see Sutyrin and Flierl (1994)), and as the mean propagation of the vortices studied above is indeed quite close to the propagation speed of long vortical waves here (Eq. (23) yields $C \simeq 0.5$ cm/s), we wondered if this was not a general result. This is the subject of the following section.

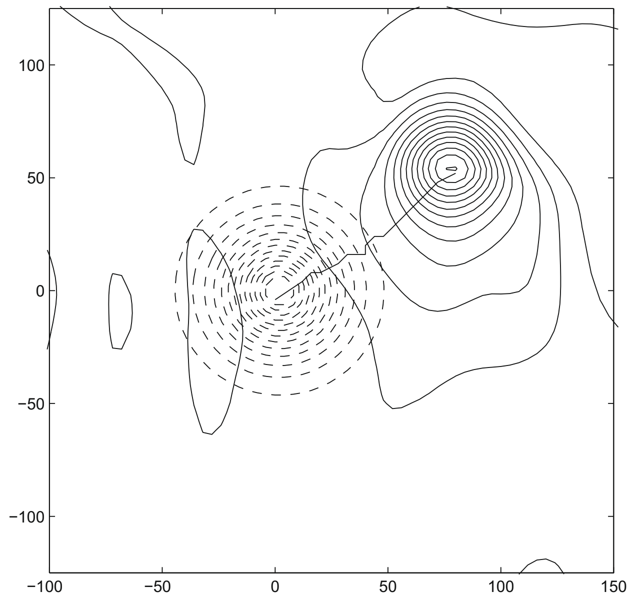

Fig. 17. Initial and final PVA in layer 1 together with the vortex trajectory. The vortex structure is similar to the reference experiment (Fig. 4), but with H_1 = 100 m, H_2 = 900 m.

5.4. Influence of the background stratification

To test if vortices propagate at the long wave speed, we have simply varied the stratification (H_1 and H_2, the density jump between the layers has been kept constant). Fig. 17 shows results with $H_1 = 100$ m and $H_2 = 900$ m (experiment "var9"). Notice that in this case $U_{Ek} = 5$ cm/s so that the net displacement of tracers located in the upper layer after 100 days would be L $\simeq$ 432 km. The long wave propagation speed is however, unchanged in comparison with all previous experiments: $C = 0.5$ cm/s. The vortex displacement is 80 km cross wind (corresponding to a propagation speed $C \simeq C = 0.9$ cm/s), and 52 km along wind, drastically different from all previous cases and from both the Ekman drift and long wave limit. Also note the strong deformation of the vortex in this case.

Fig. 18 shows the results with $H_1 = 500$ m and $H_2 = 1500$ m (experiment "var10"). Notice that in this case $U_{Ek} = 1$ cm/s as in the reference experiment but the long wave propagation speed is half the one of the previous experiments: $C = 0.25$ cm/s. We find a cross wind displacement of 32 km (corresponding to a propagation speed $C \simeq C = 0.37$ cm/s), and an along wind displacement of 20 km.

These results show that vortices do not propagate at the long wave limit and suggests that there is no simple formula to calculate the propagation of vortices under the influence of a wind stress. It however, confirms the strong compensating impact of the beta-gyre on the transport of water masses by surface vortices.

6. Summary and discussion

In this paper we have revisited and extended the effect discovered in Stern (1965). We have confirmed that the wind stress can interact with vortical structures. We have shown in particular that for vortices a dipolar PVA is generated which is associated with dipolar circulations in the vortex core that inhibits the Ekman drift for surface vortices, as expected from the linear theory, but also induces along-wind displacements. This process also induces propagation of subsurface vortices (in the direction of the Ekman drift this time), even though their cores are located below the region influenced by Ekman currents.

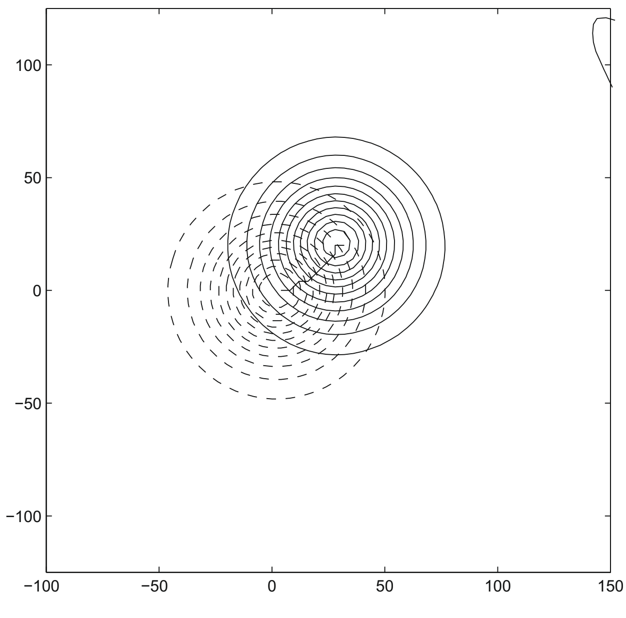

Fig. 18. Initial and final PVA in layer 1 together with the vortex trajectory. The vortex structure is similar to the reference experiment (Fig. 4), but with $H_1 = 500$ m, $H_2 = 1500$ m.

The dipolar PVA structure has been calculated as a function of the vortex rotation rate and stratification.

For the reference configuration chosen here, we have only found a weak sensitivity to the vortex radius and strength. But further tests have shown that there does not exist a simple rule to evaluate the propagation speed, so that we can not state that the observed weak influence of the vortex strength or radius is general. The effect of the vortex deformations have to be taken into account to evaluate the displacement analytically.

For linear vortical waves, Stern (1965) found that the propagation speed is a simple function of the background stratification and wavelength. Stern (1965) formula has been reproduced in the simplified two-layer configuration considered here. Its extension to more realistic configurations with many layers is straightforward, and could be tested to explain some discrepancies between observations of Rossby wave propagation speeds and their evaluations from theory, as this effect has not been taken into account up to now to our knowledge.

In oceanic global circulation models, used to study climate evolution for instance, the resolution is generally not eddy resolving and the effect studied here is thus not taken into account. The influence of the Ekman drift on the transport of surface and subsurface water masses, and overturning circulation, could thus be strongly biased, at least if it is mostly associated with the propagation of vortices. In this respect, Hallberg and Gnanadesikan (2006) is particularly interesting: this study has compared coarse resolution to eddy-resolving models and the authors have found a strong effect of the presence of eddies on the transport of water masses at large scale. Even though it is not easy to connect both studies in details, the latter result is consistent with the present and some former studies, which show that coherent vortices have a very particular behavior when they interact with their environment, and are not simply advected by background currents as would be inert ("non vortical") particles.

The displacement of coherent vortices is indeed a function of the planetary and topographic beta-effect, large scale geostrophic circulation, Ekman drift, and self propagation depending on the vortex structure (see for instance Morel and McWilliams, 1997). Among all the previous mechanisms, only advection by large scale geostrophic currents and Ekman drift can be represented in non-eddy resolving models, so that we can only expect the latter to accurately represent the water mass transport and general stratification of the ocean if these processes are dominant.

We, however, now know that a significant, if not major, fraction of the transport of water masses is done through coherent vortices (see Hallberg and Gnanadesikan (2006) and references therein). In (Vandermeirsch et al., 2001) we have shown that large scale geostrophic circulation is expected to have a moderate impact, as only the barotropic component has an influence on the propagation of coherent vortices, and we have here shown that vortices have again very peculiar propagation when interacting with a wind stress. According to the present study, the Ekman drift should indeed be drastically reduced for surface eddies and enhanced for subsurface eddies. Therefore, in addition to the missing mechanisms (planetary beta-effect, self propagation, ...), this specific behavior of oceanic vortices when interacting with large scale geostrophic flows or wind stress is another reason to expect strong differences between coarse resolution and eddy-resolving models, even if advection by large scale geostrophic currents and Ekman transport were dominant processes.

A specific parameterization, representing the effect of the transport by coherent vortices, could be developed for coarse resolution models. The usual coarse resolution parameterization assumes that vortices tend to propagate so as to reduce horizontal gradients of buoyancy and represent their effect as a diffusion of this quantity. But the numerous mechanisms at stake for the dynamics of oceanic vortices and their complexity makes it difficult, if possible at all, to develop a general parameterization. In the present study, we have for instance been unable to find simple rules to describe a general effect of the wind stress on the propagation of eddies, and this wind induced propagation does not necessarily act so as to reduce buoyancy gradients.

As a result, eddy-resolving models may be the only way to accurately model the overturning circulation, large scale stratification and climate evolution in general.

We also believe the process studied here could have some other interesting impacts in particular on the development of baroclinic/barotropic instability. Apart from the direct modification of the PVA structure of currents studied in Thomas (2005), Morel et al. (2006) or Thomas and Ferrari (2008), the process studied here is also able to modify the propagation speed of vortical waves and could play a role in the scale selection and growth rate of the instability.

It is important to keep in mind that the configuration we have used for our study is very specific. The generalisation of our results to more realistic configurations must then be cautiously evaluated. However, we believe that the convergence of our approach with what was found in Stern (1965), who did consider the details of the mixed layer dynamics, the fact that the PVA generation mechanism is still valid with a sophisticated mixed layer dynamics (Thomas, 2005; Thomas and Ferrari, 2008), and the consistency between our results and what has been found inHallberg and Gnanadesikan (2006), suggest the present results indeed extends to realistic configurations.

Finally, let us mention that other non-linear effects of a wind stress on the propagation of vortices have been studied previously and could further influence the dynamics and propagation of vortices. In particular Dewar and Flierl (1987) have studied the effect of the sea surface velocity and temperature on the dynamics of a Gulf-Stream ring when interacting with the wind and have found that it indeed had an influence on their cross wind propagation.

Acknowledgement

This study is a contribution to SHOM project MOUTON funded by DGA (PEA012401) and the French Navy. The authors gratefully acknowledges Prof. Xavier Carton, Dr. Robert Hallberg and two reviewers whose criticisms, knowledge of the existing literature, and careful reading greatly helped improving the manuscript.

References

Bleck, R., Boudra, B., 1986. Wind-driven spin-up eddy-resolving ocean models formulated in isopycnic and isobaric coordinates. J. Geophys. Res., 7611–7621.

Bleck, R., Rooth, C., Hu, D., Smith, L., 1992. Salinity driven thermocline transients in a wind and thermohaline forced isopycnic coordinate model of the North Atlantic. J. Phys. Oceanogr. 22, 1486–1505.

Bleck, R., Smith, L., 1990. A wind-driven isopycnic coordinate model of the north and equatorial Atlantic Ocean 1. Model development and supporting experiments. J. Geophys. Res., 3273–3285.

Carton, X., 2001. Hydrodynamical modeling of oceanic vortices. Surv. Geophys. 22 (3), 179–263.

Carton, X., 2008. Oceanic Vortices. Fronts, Waves and Vortices. Springer Verlag. Chapter 3.

Carton, X., McWilliams, J., 1989. Barotropic and baroclinic instabilities of axisymmetric vortices in a qg model. Mesoscale/Synoptic Coherent Structures in Geophysical Turbulence Elsevier, 225–244.

Cushman-Roisin, B., 1994. Introduction to Geophysical Fluid Dynamics. Prentice-Hall Inc.. pp. 320.

Dewar, W.K., Flierl, G.R., 1987. Some effects of the wind on rings. J. Phys. Oceanogr. 17, 1653–1667.

Dewar, W.K., Meng, H., 1995. The propagation of submesoscale coherent vortices. J. Phys. Oceanogr. 25, 1745–1770.

Ekman, V., 1905. On the influence of the earths rotation on ocean currents. Arkiv. Mat. Astron. Fysik. 2 (11), 1–53.

Hallberg, R., Gnanadesikan, A., 2006. The role of eddies in determining the structure and response of the wind-driven southern hemisphere overturning: results from the meso project. J. Phys. Oceanogr. 36, 2232–2251.

Herbette, S., Morel, Y., Arhan, M., 2003. Erosion of a surface vortex by a seamount. J. Phys. Oceanogr. 33, 1664–1679.

Herbette, S., Morel, Y., Arhan, M., 2005. Erosion of a surface vortex by a seamount on the beta plane. J. Phys. Oceanogr. 35, 2012–2030.

Hogg, N., Stommel, H., 1990. How currents in the upper thermocline could advect meddies deeper down. Deep-Sea Res. 37, 613–623.

Hoskins, B., McIntyre, M., Robertson, W., 1985. On the use and significance of isentropic potential vorticity maps. Quart. J. Roy. Meteor. Soc. 111, 877–946.

Ito, Y., Kubokawa, A., 2003. Southward translation of strongly nonlinear warm eddies in a 2 1/2-layer beta-plane model. J. Phys. Oceanogr. 33, 1250–1273.

Morel, Y., 1995. The influence of an upper thermocline current on intrathermocline eddies. J. Phys. Ocean 267, 23–51.

Morel, Y., Darr, D., Tailandier, C., 2006. Possible sources driving the potential vorticity structure and long-wave instability of coastal upwelling and downwelling currents. J. Phys. Ocean 36, 875–896.

Morel, Y., McWilliams, J., 1997. Evolution of isolated interior vortices in the ocean. J. Phys. Ocean 27, 727–748.

Morel, Y., McWilliams, J., 2001. Effects of isopycnal and diapycnal mixing on the stability of oceanic currents. J. Phys. Ocean 31, 2280–2296.

Pedlosky, J., 1987. Geophysical Fluid Dynamics. Springer, New York. pp. 710.

Richardson, P., Walsh, D., Armi, L., Schroder, M., Price, J., 1989. Tracking three meddies with sofar floats. J. Phys. Oceanogr. 19, 371–383.

Stern, M., 1965. Interaction of a uniform wind stress with a geostrophic vortex. Deep-Sea Res. 12, 355–367.

Sutyrin, G., Flierl, G., 1994. Intense vortex motion on the beta-plane: development of the beta gyres. J. Atmos. Sci. 51, 773–790.

Sutyrin, G., Morel, Y., 1997. Intense vortex motion in a stratified fluid on the beta-plane. An analytical model and its validation. J. Fluid Mech. 336, 203–220.

Thomas, L.N., 2005. Destruction of potential vorticity by winds. J. Phys. Oceanogr. 35, 2457–2466.

Thomas, L.N., Ferrari, R., 2008. Friction, frontogenesis, and the stratification of the surface mixed layer. J. Phys. Oceanogr. 38, 2501–2518.

Vandermeirsch, F., Morel, Y., Sutyrin, G., 2001. The net advective effect of a vertically sheared current on a coherent vortex. J. Phys. Oceanogr. 31, 2210–2225.

Winther, N., Morel, Y., Evensen, G., 2007. Efficiency of high order numerical schemes for momentum advection. J. Mar. Sys. 67, 31–46.